ADVANCED MATERIALS INTERFACES
www.advmatinterfaces.de

UV Direct Write Metal Enhanced Redox (MER) Domain Engineering for Realization of Surface Acoustic Devices on Lithium Niobate

Didit Yudistira, Andreas Boes, Amgad R. Rezk, Leslie Y. Yeo, James R. Friend, and Arnan Mitchell*

A new and highly versatile domain patterning method—ultraviolet direct write metal enhanced redox (UV direct write MER)—achieves deep domains with practically no thermally-induced damage on the surface of lithium niobate crystals. In UV direct write MER, after coating with a thin layer of chromium, the domain inversion is generated by a redox process induced in the crystal by illumination with high intensity UV in an ambient dry nitrogen atmosphere. This new technique enables the fabrication of practical piezoelectric acoustic superlattice structures on 128° YX-cut $LiNbO_3$, the most widely used crystal cut for surface acoustic wave applications. For example, UV direct write MER was used to form an acoustic superlattice 128° YX structure that in turn enabled the generation of surface acoustic waves of sufficient strength to develop fluid flow within a droplet of water, demonstrating its potential in practical microfluidic manipulation. This is the first demonstration of a UV direct write surface acoustic wave transducer reported to date, made possible only due to the unique qualities of the MER domain engineering process.

1. Introduction

The ability to integrate surface acoustic waves (SAWs) into microdevices have opened a new frontier in a wide range of fields, from electronics,[1] optical communications,[2] and biosensors[3–5] to acoustic microscopy[6] and gyroscopics.[7] Recently, the use of SAW for manipulation of fluids and bioparticles at small scales has been demonstrated for point-of-care diagnostics, high throughput drug screening and drug delivery, all of which have received significant interest.[8] Typically, transducers based on interdigital electrodes deposited on a single crystal of piezoelectric material such as lithium niobate ($LiNbO_3$)[9] have been used to generate and detect the SAW, particularly for applications in microfluidics.[8] A significant drawback in current approaches is the absence of accurate control of the SAW propagation and behavior; far more care is necessary in forming structures that can generate, detect, and manipulate the SAW. To do so, structures including acoustic waveguides[10] and metal gratings[1] have been employed in telecommunications and optical applications to enable lateral confinement[11] and wavelength selection of SAW and acoustic mirrors.[1] While metal gratings, including interdigital transducers, have found broad acceptance, high fabrication resolution in the metal film's structure is required, particularly in the finger electrode structure, which can be difficult to fabricate, and subject to substantial damage when used for high power applications.[12] Further, the metal can significantly disturb the acoustic waves' generation, form parasitic modes and overtone resonances, and suppress their departure from the electrode structure on the surface, all critical to the device's application.

An alternate means of generating and detecting the SAWs is through the use of a piezoelectric acoustic superlattice (ASL).[13,14] An ASL is an engineered structure that is similar to periodically poled lithium niobate in nonlinear optics;[15] however, instead of a periodic change in the sign of the second-order optical nonlinearity, the structure possesses an alternating change in the sign of the piezoelectric constant. Uniform fields can then be applied using coplanar electrodes on either side of the ASL, resulting in a periodic displacement of the surface and hence the generation of the SAW.[13,14] In previous work,[16] we have shown an ASL can induce a SAW bandgap similar to phononic structures physically patterned on the substrate surface,[17,18] but absent the structure required in traditional phononic devices that may interfere with the SAW and its application. Piezoelectric ASLs have since been used to achieve a monolithic, integrated SAW in addition to bulk acoustic wave devices,[14,19] acousto-optic filters,[20,21] delay lines,[14,22] and phonon-polariton crystals.[23–25]

Dr. D. Yudistira, A. Boes, Prof. A. Mitchell
School of Electrical and Computer Engineering
RMIT University
Melbourne, VIC 3001, Australia
E-mail: didit.yudistira@rmit.edu.au
A. R. Rezk, Prof. L. Y. Yeo
Micro/Nanophysics Research Laboratory
RMIT University
Melbourne, VIC 3001, Australia
Prof. J. R. Friend
Micro/Nanophysics Research Laboratory
RMIT University, Melbourne
VIC, 3001, Australia
The Melbourne Centre for Nanofabrication
Clayton, VIC 3166, Australia

DOI: 10.1002/admi.201400006

To date, the ASL structures have used ad-hoc electric field poling on a single crystal of Z-cut $LiNbO_3$.[15] While these show considerable potential, there is an inherent limitation of this crystal cut in that it is difficult to generate surface waves without also generating bulk waves. For applications where concentrated SAW energy is required, for example in microfluidic actuation,[8] the substrate of choice is 128° YX-cut $LiNbO_3$, as it possesses an optimal coupling constant and also suppresses parasitic bulk waves.[26] However, it is not possible to create an ASL on 128° YX-cut $LiNbO_3$ using ad-hoc electric field poling, as the polar axis is not aligned to a vertical axis of the wafer. While alternate techniques for domain engineering of non-polar cut $LiNbO_3$ have been reported, including Ti diffusion[27] and oxygen out-diffusion,[27,28] the diffusive nature of these processes makes it difficult to achieve the micrometer-scale, fine-featured structures necessary to achieve the requisite acoustic frequencies. Recently, a direct write process using a continuous wave UV laser has been demonstrated as a means for domain engineering[29,30] the non-polar facets of ferroelectric crystals, such as X- and Y-cut $LiNbO_3$[30] and also strontium barium niobate (SBN).[31] A significant advantage of this technique is that local domain inversion can be achieved at room temperature by directly scanning the UV laser across the crystal surface, providing superior domain patterning control useful in creating complex poling structures on facets of an arbitrary polarization orientation. However, to achieve domains on the order of a few microns deep, the intensities and durations of laser exposure required typically lead to thermally-induced damage on the surface of the crystal.

In this paper, we present a new and highly versatile domain patterning method—UV direct write metal enhanced redox (MER)—that we show to be effective for the patterning of piezoelectric ASL structures on 128° YX-cut $LiNbO_3$. This new technique achieves domain engineering by energizing a thin film of chrome on the surface of the $LiNbO_3$ crystal using a focused UV beam in a dry nitrogen atmosphere. The energized chrome drives a redox process and the subsequent movement of defect ions causes domain inversion beneath the irradiated regions. To demonstrate the utility of this technique, we fabricated an ASL structure and employed it as a SAW transducer. Prior to fabrication we carried out finite element simulation to predict the SAW generation as a function of the depth of the MER-made ASL structure. The functionality of this device was then validated through a brief demonstration of microfluidic actuation. This is the first demonstration of a UV direct write SAW transducer reported to date and is only possible due to the unique qualities of the MER domain engineering process. The ability to flexibly create practical ASL structures at room temperature on demand and on arbitrary crystal orientations is anticipated to open a new frontier in SAW device research and applications.

2. Results and Discussion

2.1. Domain engineering 128° YX-cut $LiNbO_3$ with UV Direct Write MER

The fabrication setup is illustrated in **Figure 1**a. A 128° YX congruent $LiNbO_3$ wafer with a thickness of 500 µm (Roditi Ltd., London, UK) was coated with a 40 nm chromium film by e-beam evaporation, followed by irradiation by a 7 µm diameter UV beam generated with a frequency doubled argon ion laser with a wavelength of 244 nm. The beam was tightly focused using a fused silica lens with a focal length of 40 µm. The sample was then positioned in a closed chamber with a fused silica window. The chamber was filled with dry nitrogen and mounted on a three-axis computer-controlled translation stage that moves at a velocity of 0.1 mm/s, scanning a focused UV laser beam across the surface of the substrate along a direction perpendicular to the crystallographic *X*-axis (Figure 1a). To determine the achievable domain depth, the intensity of the UV beam I was increased from 2.6×10^5 W cm^{-2} to 3.4×10^5 W cm^{-2}. After the UV irradiation process, the chromium was removed from the surface sample using a chromium etchant (Figure 1b). To analyze the profile and also the depth of the resulting UV written domains, the samples were diced along the *X*-axis and polished at an angle $\theta = 6°$ as shown in Figure 1c. The angle-polished samples were treated with hydrofluoric acid (HF), which preferentially etched the domain-inverted crystal. The etched, angle-polished surface was imaged using scanning electron microscopy (SEM), in which the sample was positioned with its thickness parallel to the electron beam direction. For comparison, we also performed UV direct write domain engineering on uncoated crystals, obtaining results for these uncoated samples similar to previous reports.[30]

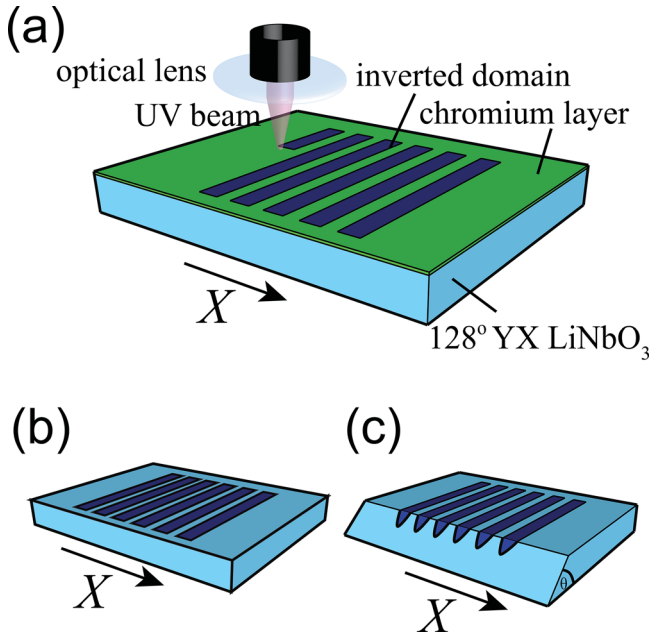

Figure 1. (a) Illustration of the UV poling fabrication setup used to fabricate the ASL structure in which the domain is written by a focused UV laser moved along a direction perpendicular to the crystallographic *X*-axis of the crystal. Prior to the writing, the $LiNbO_3$ crystal was covered with a 40 nm thick chromium layer. (b) After the process, the chromium was removed from the sample using chromium etchant. (c) The domain the sample was then diced along *X*-axis and polished at an angle $\theta = 6°$. Subsequent etching using HF was performed to reveal the resulting domain.

Microscope images taken from the coated samples, after removal of the chromium layer, and of the uncoated samples, are shown in **Figures 2**a and 2b, respectively. Figure 2a clearly

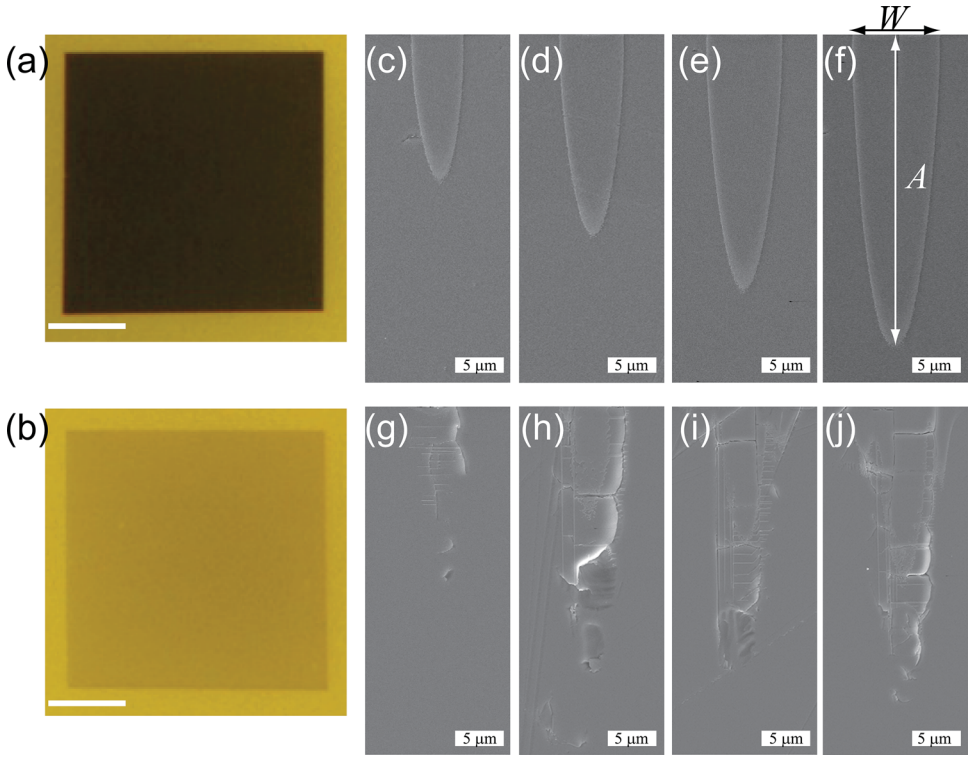

Figure 2. Micrographs of (a) coated and (b) uncoated samples taken after the UV irradiation process. For the coated sample, the image (a) was taken after removal of the chromium layer. The scale bars in (a) and (b) are 1 mm. (c-f) SEM images of the resulting domains that were obtained using UV direct write MER with various UV beam intensities *I*: (c) 2.6×10^5 W cm^{-2}, (d) 2.9×10^5 W cm^{-2}, (e) 3.1×10^5 W cm^{-2}, and (f) 3.4×10^5 W cm^{-2}. (g-f) SEM images of the resulting domains obtaining using a standard UV domain writing process with various intensities: (g) 2.6×10^5 W cm^{-2}, (h) 2.9×10^5 W cm^{-2}, (i) 3.1×10^5 W cm^{-2}, and (j) 3.4×10^5 W cm^{-2}.

shows that the UV illuminated area on the coated sample is much darker in color than the uncoated sample (Figure 2b), indicating that a redox process has occurred on the crystal surface.[32] This process can be explained as follows: the chromium film absorbs the UV light and heats rapidly, locally heating both the chromium and the $LiNbO_3$ crystal. At this elevated temperature, the oxygen in the $LiNbO_3$ crystal becomes mobile and can out-diffuse from the surface.[32] The temperature also enhances the reactivity of the chromium, such that it becomes a strong sink for the out-diffusing oxygen. The UV irradiation is conducted in an oxygen deficient nitrogen atmosphere and so only the oxygen from the $LiNbO_3$ crystal diffuses into the chromium where it is trapped. This continues until the chromium is saturated, becoming fully oxidized; or until the localized heating due to irradiation is halted.

It has been reported that oxygen out-diffusion, as seen in Figure 2a, can cause domain inversion.[32] To visualize the domain polarity, the samples were cross-sectioned, polished at 6° and then etched in HF. The etched surfaces were inspected using SEM, as shown in Figures 2c-f, revealing the domain structure of the chrome-coated samples for various laser intensities. Equivalent images of the uncoated samples are presented in Figures 2g-j. Figures 2c-f clearly show that domain inversion has been achieved with the UV direct write MER process and that the depth and width of the domains increase with higher UV light intensities with no damage apparent on the surface. While the results for the uncoated samples (Figures 2g-h) also reveal inverted domains that are enlarged with the UV intensity, there is nevertheless evidence of significant damage (cracks) on the domains even at the lowest intensity (Figure 2g).

Given that the samples were polished at an angle $\theta = 6°$, the domain depth presented in the SEM images appears stretched. The actual domain depth can be determined using $\delta = A \tan \theta$, where A is the depth measured from the SEM image (see Figure 2f). **Figures 3**a and 3b present the domain depth δ and width W as a function of the laser intensity I. It can be seen that both the depth and the width increase almost monotonically, although the depth increases slightly more rapidly than the width. This ability to control both the width and the depth could be very useful for the fabrication of the piezoelectric superlattice structure, as it would allow flexible control of the duty cycle and the period of the lattice. In our experiments, we observed that damage or cracks on the domain started to become apparent even on the coated samples when the UV intensity was at or above 3.4×10^5 W cm^{-2}.

2.2. Impact of Domain Depth of the MER Generated 128° YX ASL Structure on the Generation of the SAW

To demonstrate the capabilities of UV direct write MER, we used the process to fabricate a piezoelectric acoustic superlattice (ASL) structure in 128° YX-cut $LiNbO_3$ for use as a SAW transducer. All previously demonstrated ASL SAW transducers

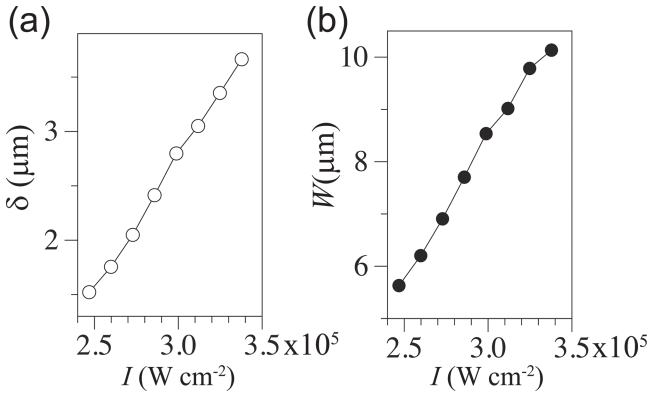

Figure 3. (a) Measured domain depth δ and (b) width W as a function of the intensity UV beam I from the samples, which were patterned with UV direct write MER.

have been achieved on Z-cut crystals with the engineered domains extending through the entire thickness of the crystal substrate.[13,14,19] It is clear from Figure 2 that while the domains are formed with MER, their depth is finite at several microns deep. Thus, before fabricating the ASL, we first investigated the impact of the domain depth on the generation of the SAW using a finite element simulation. **Figure 4**a illustrates the actual three-dimensional structure of the ASL SAW transducer.[13] The simplified two-dimensional model considered consisted of the cross-section along the red dashed line shown in Figure 4b, with a domain depth δ and period Λ, surrounded by perfectly matched layers (PML) at the boundaries of the numerical domain. The simplified model therefore only considers the influence of the vertical component of the electric field on the generation of the SAW. The depth of the domain was normalized using a dimensionless parameter $\tau = \delta/\Lambda$. Figure 4c shows the calculated spectral response of the transducer at $\tau = 0.3$ from which a resonance peak at frequency $f_{SAW} = V_{SAW}/\Lambda$ was observed where V_{SAW} is the SAW velocity, indicating the expected SAW generation. This was also confirmed by the corresponding displacement profile shown in Figure 4d, calculated at f_{SAW}. Figure 4e presents the calculated full SAW displacement profile of the transducer at $\tau = 0.3$, obtained from the three-dimensional finite element simulation[13] by considering all components of the electric field. This result shows that the energy is confined between the electrodes, in contrast to the previous ASL transducers realized on Z-cut crystal substrates along which the acoustic wave leaks beneath the metal electrodes[13,33] unless confined by an acoustic waveguide formed by mass loading.[19]

Having shown that SAW generation is possible even with domains that are relatively shallow ($\tau = 0.3$), we then examined the possibility of identifying an optimum domain depth by employing the two-dimensional simulation above. The frequency was fixed at the resonance (f_{SAW}), and the normalized depth τ was varied from 0 (unpoled substrate) to a large value ($\tau = 3$ in this study). For each value of τ, the transmission T was then calculated from the ratio of the outgoing SAW displacement σ_{out} to the maximum displacement σ_{max}. **Figure 5**a shows the results obtained from the numerical simulation. A maximum in the SAW transmission was obtained at around $\tau = 0.3$, implying that a freely propagating SAW should be generated by an ASL with this depth. The SAW displacement distribution for the ASL transducer with $\tau = 0.3$ is presented in Figure 5b, clearly showing the propagating nature of the SAW. However, when $\tau >> 0.3$, the transmission is observed to decrease despite the generation of the SAW, suggesting that the SAW is mostly localized within the lattice. The SAW displacement pro-

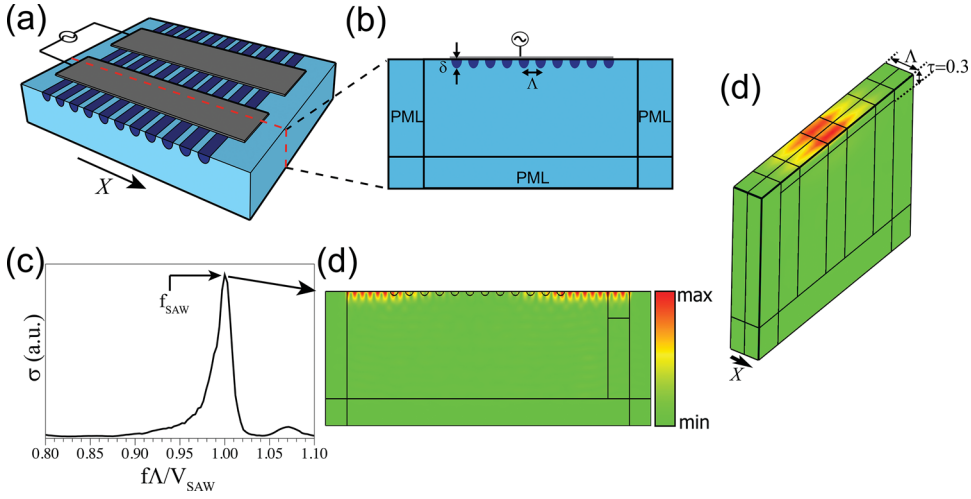

Figure 4. (a) Schematic of the ASL-based SAW transducer consisting of two coplanar electrodes acting as bus bars and the ASL structure with shallow domain depth obtained through UV direct writing. (b) Cut-out illustrating the two-dimensional model structure used in the simulation carried out along the red dashed-line shown in (a). PML refers to the perfectly matched layer applied at the domain boundaries in the simulation to match the experimental situation in which unwanted reflection is absorbed at the boundaries. (c) Calculated SAW spectral response of the transducer for a domain depth $\delta = 0.3\Lambda$. $V_{SAW} = 3980$ m/s is the SAW velocity on 128° YX-cut $LiNbO_3$. (d) Corresponding SAW displacement profile calculated at frequency f_{SAW}, verifying the generation of the SAW. (e) Calculated full displacement profile of the SAW generated on a finite depth 128° YX piezoelectric superlattice transducer. The SAW field is mostly confined within the gap region. In the calculation, the electrode gap was taken to be Λ and the electrode width is 1.5Λ.

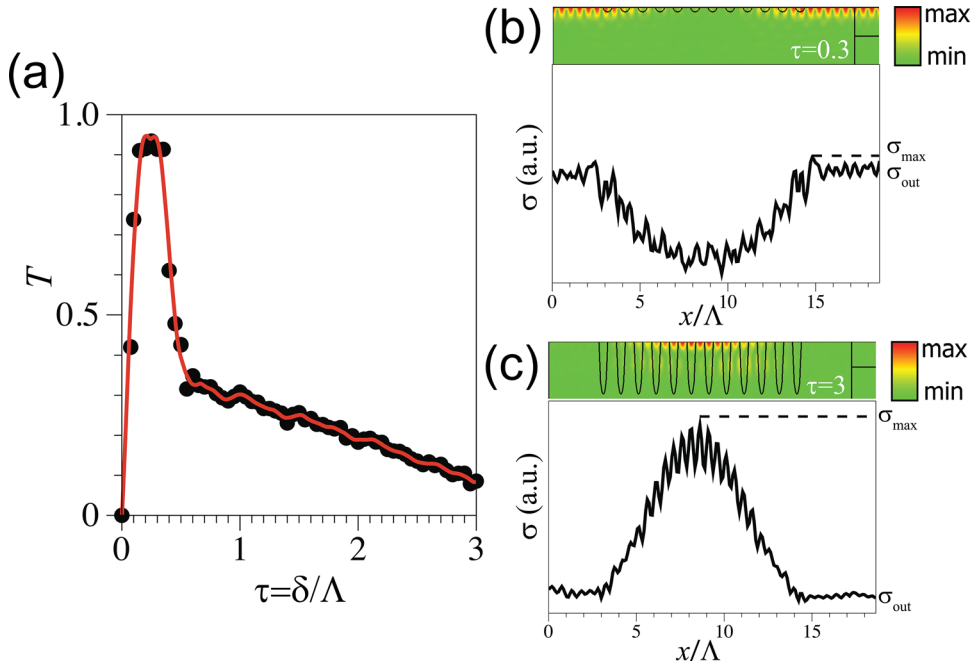

Figure 5. (a) Calculated outgoing surface acoustic energy T as a function of the domain depth δ represented by the normalized parameter τ, which was varied from $\tau = 0$ (un-written) to 3 (deeply written). The frequency was fixed at f_{SAW} in the simulation. (b) SAW displacement profile calculated at the maximum transmission $\tau = 0.3$, showing a freely propagating SAW. (c) Calculated SAW displacement profile for the case of a deeply written domain $\tau = 3$, showing the localization of the SAW.

file calculated at $\tau = 3$ and presented in Figure 5c, on the other hand, clearly indicates the stationary, bound nature of the generated SAW. This result, in fact, is in good agreement with our previous studies on Z-cut ASL structures[16] where the localization is due to the presence of a SAW band gap that induces SAW reflection, which appears to be stronger when the domain depth is larger than the lattice period. As expected, when the domain depth is insufficient ($\tau < 0.1$), it is predicted that no SAW generation should be observed.

2.3. Fabrication of Piezoelectric Acoustic Superlattice on 128° YX $LiNbO_3$ and Application of the SAW Device for Microfluidic Manipulation

Based on the above modeling results and the structures shown in Figure 2, we fabricated two ASL structures with $\Lambda = 15.5$ µm and 21 µm using MER with a laser intensity of 3.4×10^5 W cm^{-2} on a 128° YX-cut crystal substrate. The measured domain depth was around 3.4 µm, about 22% and 16% of $\Lambda = 15.5$ µm and 21 µm, respectively; thus it should be sufficiently large to generate SAWs, as suggested by the simulations in Figure 5a. Based on these values of Λ for the periods and assuming an acoustic velocity of 3980 m/s, the expected resonance frequencies f_{SAW} of the generated SAWs are 256.7 MHz and 189.6 MHz, respectively, and the structures consequently comprise 1000 periods. A pair of 150-nm thick coplanar aluminum electrodes, 80 µm in width with a 20 µm gap between them, were deposited on top of each structured substrate as shown in **Figure 6**a. The spectral response of the fabricated device was analyzed by measuring the displacement σ using a Laser Doppler Vibrometer (LDV) as a function of the frequency of the RF signal applied to the electrodes. Figures 6b and 6c show the measured acoustic displacement as a function of the applied RF frequency for ASL transducers with periods $\Lambda = 15.5$ µm and 21 µm, respectively. Strong resonances are observed around 256.8 MHz and 189.7 MHz, which are close to the expected values, and therefore verify the generation of the SAW.

To demonstrate that these MER-realized ASL structure for transducers can produce sufficient SAW amplitudes to perform useful work, we conducted a proof-of-concept microfluidic experiment to show the possibility of acoustically manipulating a particle suspension within a sessile droplet, similar to what has been done using IDT-based SAW devices on 128° YX-cut $LiNbO_3$[34] for comparison. Briefly, a 3 µl droplet in which 4.5 µm fluorescent polystyrene microparticles were suspended was centered on the $\Lambda = 15.5$ µm transducer, as shown in **Figure 7**a. The transducer was driven by applying an RF signal at its resonance frequency $f_{SAW} = 256.8$ MHz and at a power of 3 W, generating SAW with a displacement $\sigma = 0.1$ nm as measured with the LDV, corresponding to a vibration velocity of 0.16 m/s. The particles inside the droplet were imaged as shown in Figures 7b and 7c, respectively, before and 30 seconds after commencing the electrical drive of the transducer. Figure 7c shows a vortex flow pattern arising from acoustic (Eckart) streaming in the drop induced by the SAW that is typical of standard IDTs.[34] We note from the figure that the flow pattern starts from the center of the droplet corresponding to the aperture of the SAW field in the gap region, as previously shown in the simulation (Figure 4e). As such, it is not difficult to surmise that the ASL structure fabricated in the present work is capable of generating SAWs that can interact with fluids and

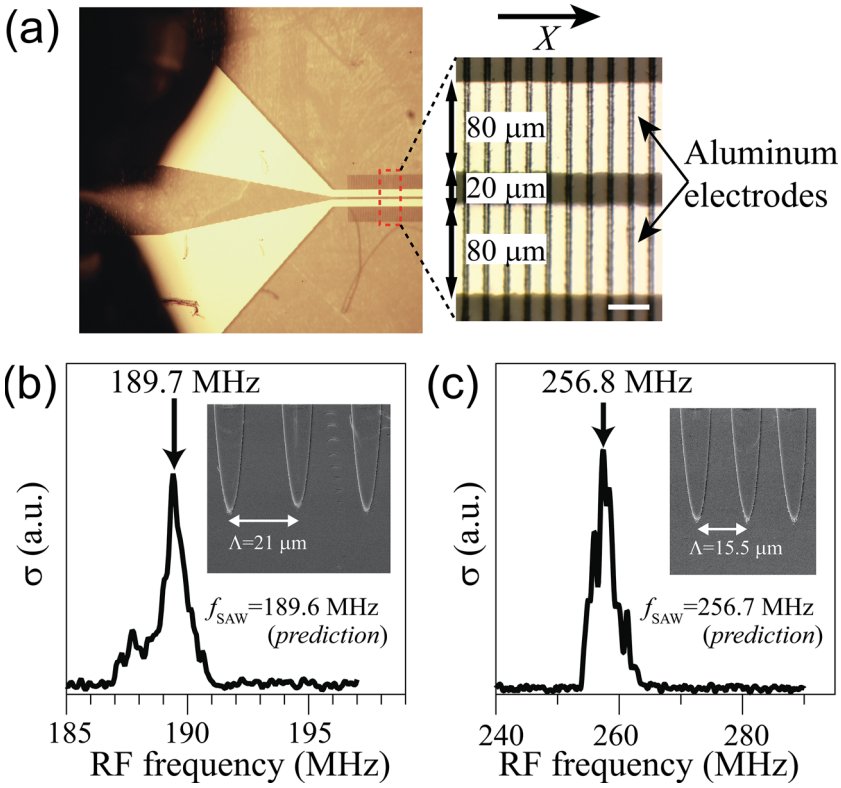

Figure 6. (a) Micrograph of the fabricated 128° YX-cut ASL transducer fabricated with UV direct write MER with $I = 3.4 \times 10^5$ W cm^{-2} with the width and the gap of the aluminum electrodes being 80 μm and 20 μm, respectively. (b,c) Measured spectral responses of the transducer for periods $\Lambda = 21$ μm and 15.5 μm, respectively. The insets in (b,c) show the SEM images of the ASL structures with different periods Λ. The scale bar in (a) is 20 μm.

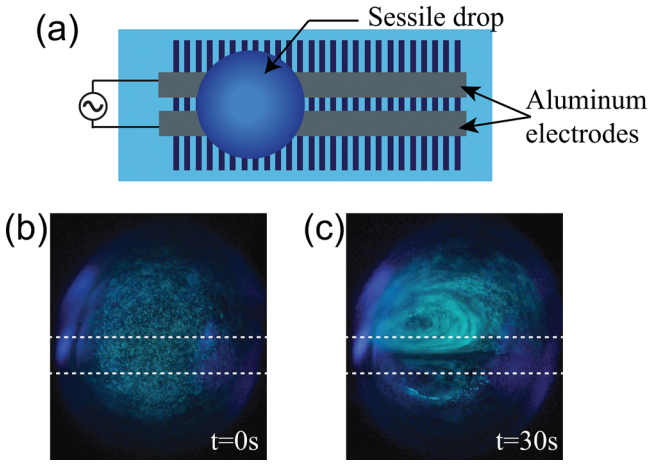

Figure 7. (a) Schematic of the experimental setup in which the SAW generated using the 128° YX-cut ASL transducer is transmitted into a sessile fluid drop placed on the transducer surface. (b) Image showing the distribution of polystyrene microparticles suspended in the drop in the absence of SAW. (c) Image showing the distribution of polystyrene microparticles suspended in the drop 30 seconds after the ASL was driven, showing the possibility for driving SAW-driven acoustic streaming, known as Eckart flow, that is typical of the behavior observed when the droplet is excited with the SAW generated from conventional IDTs. In (b) and (c), the dashed-lines indicate the outer edges of the coplanar electrodes.

can be used to effect the entire range of SAW microfluidic processes (e.g., drop actuation and microcentrifugation) driven by acoustic streaming that have thus far been reported and which have received considerable attention to date.[8] The ASL structure nevertheless retains a significant advantage of IDT structures in that it enables direct interaction between the fluid and the SAW at the point of generation without interference from the electrodes and that it enables far higher acoustic powers to be used beyond that possible with IDT structures.

3. Conclusion

In summary, we have introduced metal enhanced redox (MER) as a highly versatile UV direct write technique for domain patterning of lithium niobate that can achieve deep domains with practically no thermal-induced damage on the surface. The domain inversion, generated by a redox process that is induced in a crystal coated with a thin layer of chromium, is illuminated with a high intensity of UV beam in ambient dry nitrogen atmosphere. This new technique makes it possible to fabricate practical piezoelectric acoustic superlattice structures on 128° YX-cut $LiNbO_3$, which is the most widely used crystals cut for SAW applications. We have conducted simulations and experimental validation, which show that the ASL structure can be exploited as an effective transducer and that the generated SAW field is freely propagating and mostly confined within the gap region, which is in contrast to previously demonstrated Z-cut ASL transducers.[13,33] We subsequently showed the possibility of using the fabricated transducer for driving flow and suspended microparticles within a fluid droplet, demonstrating the platform can be exploited for practical microfluidic manipulation. The proven simplicity, flexibility and effectiveness of this technique therefore make it attractive for rapidly producing complex acousto-microfluidic devices.

4. Experimental Section

Surface acoustic wave: The SAW was generated by applying a RF signal to the transducers fabricated with UV direct write MER technique using a signal generator (Rhode & Schwarz, SML01, North Ryde, NSW, Australia) in conjunction with an amplifier (Mini Circuits ZHL-5W-1, 5–500 MHz, Brooklyn, NY, US) and 3 A, ±24 DC power supply. The spectral response of the transducer was then measured using a Laser Doppler Vibrometer (LDV, UHF-120, Polytec GmBH, Waldbronn, Germany). An acoustically absorbing material (α-gel, Geltec Ltd, Yokohama, Japan) was placed on the backside of the observed structure.

Acoustofluidics: A deionized water droplet of 3 μl suspended with 4.5 μm polystyrene particles (Sigma-Aldrich Pty Ltd, North Ryde, NSW, Australia) was placed on the transducer. The particle motion was captured using a digital SLR camera (EOS 550D, Canon, Utsnomiya,

Japan) fitted with a macro lens (EF-S, Canon; 60 mm focal length, F/2.8).

Acknowledgements

The authors would like to thank Elisabeth Soergel from the Institute of Physics, Bonn University, for fruitful discussions. L.Y.Y is grateful for funding from the Australian Research Council for an Australian Research Fellowship under Discovery Grant Project DP0985253. J.R.F is grateful to the Melbourne Centre for Nanofabrication for a Senior Tech Fellowship and to RMIT University for a Vice-Chancellor's Senior Research Fellowship, and for funding of this work in part through Australian Research Council grant DP120100013.

Received: January 3, 2014
Revised: March 28, 2014
Published online: April 15, 2014

[1] D. Morgan, Surface Acoustic Wave Filters, Second Edition: *With Applications to Electronic Communications and Signal Processing*; 2nd ed.; Academic Press, Oxford, UK, **2007**.
[2] W. Sohler, H. Hu, R. Ricken, V. Quiring, C. Vannahme, H. Herrmann, D. Büchter, S. Reza, W. Grundkötter, S. Orlov, H. Suche, R. Nouroozi, Y. Min, *Opt. Photonics News* **2008**, *19*, 24.
[3] D. S. Ballantine, Jr., R. M. White, S. J. Martin, A. J. Ricco, E. T. Zellers, G. C. Frye, H. Wohltjen, *Acoustic Wave Sensors: Theory, Design, & Physico-Chemical Applications*; Academic Press, San Diego, USA, **1996**.
[4] T. M. A. Gronewold, *Anal. Chim. Acta* **2007**, *603*, 119.
[5] K. Länge, B. E. Rapp, M. Rapp, *Anal. Bioanal. Chem.* **2008**, *391*, 1509.
[6] A. Briggs, O. Kolosov, *Acoustic Microscopy*: Second Edition; Oxford University Press, New York, USA, **2009**.
[7] S. W. Lee, J. W. Rhim, S. W. Park, S. S. Yang, *J. Micromechanics Microengineering* **2007**, *17*, 2272.
[8] J. Friend, L. Y. Yeo, *Rev. Mod. Phys.* **2011**, *83*, 647.
[9] R. M. White, F. W. Voltmer, *Appl. Phys. Lett.* **1965**, *7*, 314.
[10] A. A. Oliner, *Proc. IEEE* **1976**, *64*, 615.
[11] C. H. W. Barnes, J. M. Shilton, A. M. Robinson, *Phys. Rev. B* **2000**, *62*, 8410.
[12] M. Pekarcikova, M. Hofmann, S. Menzel, H. Schrnidt, T. Gemming, K. Wetzig, *IEEE Trans. Ultrason. Ferroelectr. Freq. Control* **2005**, *52*, 911.
[13] D. Yudistira, S. Benchabane, D. Janner, V. Pruneri, *Appl. Phys. Lett.* **2009**, *95*, 052901.
[14] E. Courjon, F. Bassignot, G. Ulliac, S. Benchabane, S. Ballandras, *IEEE Trans. Ultrason. Ferroelectr. Freq. Control* **2012**, *59*, 1942.
[15] M. Yamada, N. Nada, M. Saitoh, K. Watanabe, *Appl. Phys. Lett.* **1993**, *62*, 435.
[16] D. Yudistira, A. Boes, D. Janner, V. Pruneri, J. Friend, A. Mitchell, *J. Appl. Phys.* **2013**, *114*, 054904.
[17] S. Benchabane, A. Khelif, J.-Y. Rauch, L. Robert, V. Laude, *Phys. Rev. E* **2006**, *73*, 065601.
[18] J.-H. Sun, T.-T. Wu, *Phys. Rev. B* **2006**, *74*, 174305.
[19] D. Yudistira, S. Benchabane, D. Janner, V. Pruneri, *Appl. Phys. Lett.* **2011**, *98*, 233504.
[20] D. Yudistira, D. Janner, S. Benchabane, V. Pruneri, *Opt. Lett.* **2009**, *34*, 3205.
[21] H. Gnewuch, N. K. Zayer, C. N. Pannell, G. W. Ross, P. G. R. Smith, *Opt. Lett.* **2000**, *25*, 305.
[22] R.-C. Yin, S.-Y. Yu, C. He, M.-H. Lu, Y.-F. Chen, *Appl. Phys. Lett.* **2010**, *97*, 092905.
[23] X. Hu, Y. Ming, X. Zhang, Y. Lu, Y. Zhu, *Appl. Phys. Lett.* **2012**, *101*, 151109.
[24] C. Huang, Y. Zhu, *Phys. Rev. Lett.* **2005**, *94*, 117401.
[25] Y. Zhu, X. Zhang, Y. Lu, Y. Chen, S. Zhu, N. Ming, *Phys. Rev. Lett.* **2003**, *90*, 053903.
[26] K. Shibayama, K. Yamanouchi, H. Sato, T. Meguro, *Proc. IEEE* **1976**, *64*, 595.
[27] K. Nakamura, K. Fukazawa, K. Yamada, S. Saito, *IEEE Trans. Ultrason. Ferroelectr. Freq. Control* **2006**, *53*, 651.
[28] K. Nakamura, K. Fukazawa, K. Yamada, S. Saito, *IEEE Trans. Ultrason. Ferroelectr. Freq. Control* **2003**, *50*, 1558.
[29] V. Dierolf, C. Sandmann, *Appl. Phys. Lett.* **2004**, *84*, 3987.
[30] H. Steigerwald, Y. J. Ying, R. W. Eason, K. Buse, S. Mailis, E. Soergel, *Appl. Phys. Lett.* **2011**, *98*, 062902.
[31] A. Boes, T. Crasto, H. Steigerwald, S. Wade, J. Frohnhaus, E. Soergel, A. Mitchell, *Appl. Phys. Lett.* **2013**, *103*, 142904.
[32] K. L. Sweeney, L. E. Halliburton, *Appl. Phys. Lett.* **1983**, *43*, 336.
[33] D. Yudistira, D. Janner, S. Benchabane, V. Pruneri, *Opt. Express* **2010**, *18*, 27181.
[34] M. K. Tan, J. R. Friend, L. Y. Yeo, *Lab. Chip* **2007**, *7*, 618.

